Phys. Status Solidi A **209,** No. 11, 2161–2166 (2012) / **DOI** 10.1002/pssa.201228137

physica status solidi a
www.pss-a.com
applications and materials science

Diffuse light-scattering properties of nanocracked and porous MoO_3 films self-formed by electrodeposition and thermal annealing

Yeong Hwan Ko, Ganji Seeta Rama Raju, Sunkook Kim, and Jae Su Yu*

Department of Electronics and Radio Engineering, Institute for Laser Engineering, Kyung Hee University, 446-701 Yongin, Republic of Korea

Received 1 March 2012, revised 13 June 2012, accepted 27 June 2012
Published online 23 July 2012

Keywords diffuse light scattering, electrodeposition, molybdenum trioxide, nanocracked, thermal annealing

* Corresponding author: e-mail jsyu@khu.ac.kr, Phone: +82 31 201 3820, Fax: +82 31 206 2820

We report the diffuse light-scattering properties of nanocracked and porous molybdenum trioxide (MoO_3) films deposited on indium tin oxide (ITO) coated glass as a transparent conductive oxide (TCO), caused by the enhanced light diffraction due to high surface roughness as well as narrow slit-like structures. By utilizing the electrodeposition and thermal annealing processes, the hydrous and amorphous molybdenum oxide films were changed into crystallized MoO_3 films with self-formed nanocracks and rough surface. From the theoretical analysis of the light behavior passing through the morphology of MoO_3 films, a considerable diffuse light scattering was predicted. In order to optimize the light-scattering property, the structural and optical characteristics of MoO_3 films on ITO/glass at different applied voltages were investigated. For a proper applied voltage of 2 V, widely distributed nanocracks and rough surface were observed, leading to the enhanced diffuse transmittance of 54% at $\lambda \sim 410$ nm. Additionally, the fabricated MoO_3 films on ITO/glass exhibited a more hydrophilic surface.

1 Introduction Photon management such as antireflection, light trapping, and light scattering has attracted great interest for improving the performance of optoelectronic and photovoltaic devices due to their enhanced absorption ability [1–5]. In particular, the scattered diffuse light passing through the transparent conductive oxide (TCO) has been considered to be a main issue for the improvement of the overall absorption in thin-film solar cells [6, 7]. For generating the enhanced light scattering, the surface morphology of the transparent top layer was modified by texturing the surface or employing the vertically aligned one-dimensional nanostructures, closely packed nanospheres, and micrograting structures [8–11]. In general, appropriate surface roughness acts as the scattering centers of light from the incoming sun radiation, which increases the light pathway in the thin absorbing layer. Another strategy is the use of the micrograting structures with a larger period length than the wavelength of incident light, thus enhancing the diffuse light by inducing the higher-order diffractions [11]. However, the modification of such structures required somewhat complicated fabrication procedures including wet chemical etching or dry etching process for micropatterns.

Meanwhile, the molybdenum oxides have been one of the promising materials for wide application fields such as electrochromic devices, battery electrodes, catalysis, and gas sensors due to their particular structural and optical properties [12–16]. Among various methods, good crystallized and stable molybdenum dioxide (MoO_2) or molybdenum trioxide (MoO_3) could be obtained by performing the electrodeposition and thermal annealing that are fast, simple, and cost-effective processes [17]. Furthermore, they exhibited nanocracks, porous, and transparent films with a self-formed extraordinary surface morphology when the hydrous and amorphous molybdenum oxide was crystallized by thermal annealing. Interestingly, such surface morphologies might be expected to offer efficient diffuse light scattering by narrow slit and texturing effects. In this work, we fabricated nanocracked and porous MoO_3 films on indium tin oxide (ITO) coated glass (*i.e.*, ITO/glass) by an electrodeposition method and a subsequent thermal annealing process. The light-scattering characteristics were investigated by measuring the total and diffuse transmittance spectra. For theoretical understanding, the light behavior passing through nanocracked and porous MoO_3 films on ITO/glass was

studied using the finite-difference time-domain (FDTD) simulations. The modified hydrophilic property of the sample surfaces was also explored.

2 Experimental details and simulation The nanocracked and porous MoO_3 films were grown on ITO/glass by the subsequent processes, including electrodeposition method and thermal annealing treatment. First, the ITO/glass substrates with 2 cm × 2 cm size and 0.1 cm thickness, which have ~15 Ω/square and ~80% transparency, were cleaned by acetone, methanol, and de-ionized (DI) water for 5 min at 60 °C, respectively. The electrolyte was simply prepared by dissolving the 10 mM ammonium molybdate tetrahydrate ($(NH_4)_6Mo_7O_{24} \cdot 4H_2O$), *i.e.*, analytical graded chemicals from Sigma–Aldrich, with magnetic stirring for 30 min. After that, the ITO/glass and platinum (Pt) electrodes were carefully dipped into the electrolyte solution at room temperature and then the electric field was applied so that the hydrous and amorphous molybdenum oxide films were formed on the ITO/glass. After 5 min of the electrodeposition process at different applied voltages, the samples were immediately rinsed in DI water and dried on the hotplate at 60 °C. For crystallization into the MoO_3 films, the sample was normally annealed in a furnace at 450 °C for 1 h in an air environment.

The morphology and surface properties of the fabricated samples were observed by utilizing an atomic force microscope (AFM, XE150, PSIA) and a field-emission scanning electron microscope (FE-SEM, LEO SUPRA 55, Carl Zeiss). For the thermogravimetric analysis (TGA) and differential thermogravimetric analysis (DTA), the two thermal analyzers (Q5000 IR, TA and Q600, TA) were used with the scratched hydrous molybdenum oxide from the deposited films on ITO/glass. The analysis of crystallinity was carried out by using an X-ray diffractometer (XRD, D8 Advance, Bruker) with a monochromated CuKα radiation ($\lambda = 0.154178$ nm). The total and diffuse transmittances of samples were characterized by using an UV–VIS–NIR spectrophotometer (Cary 5000, Varian) with an integrating sphere. The wettability of each sample was measured by a contact-angle measurement system (Phoenix-250, SEO).

For understanding the light behavior by theoretical analysis based on the FDTD simulations, the electric fields of the light passing through the samples were calculated. For the FDTD simulations, the complex refractive indices of glass (1.46), ITO (1.88), and MoO_3 ($1.9 + i0.15$) [18] were used and the distribution of E_y (*i.e.*, *y*-polarized electric field) was calculated by considering the incident plane wave of normalized Gaussian beam profile ($\lambda = 450$ nm) propagating forward in the *z*-direction.

3 Results and discussion Figure 1 shows the calculated distribution of E_y passing through the (a) MoO_3 film on ITO/glass, (b) MoO_3 film on ITO/glass with nanocracks of gap distance (100 nm), and (c) porous MoO_3 film on ITO/glass with nanocracks of gap distance (100 nm). Herein, the thicknesses of ITO and MoO_3 layers were fixed to 200 nm, which is a typical thickness for practical applications. For the flat MoO_3 film on ITO/glass, the light propagated straight with small diffraction at the surface of MoO_3 and boundaries between different layers. Meanwhile, the transmitted diffuse light could be observed with light interference patterns for the flat MoO_3 film with a crack on ITO/glass as shown in Fig. 1(b). This light behavior can be explained by the well-known Fraunhofer diffraction experiments in a narrow single slit [19]. When the incident light was passed through the narrow single slit, the diffraction patterns became wider by the relation of $\theta_n = \sin^{-1}(n\lambda/d)$, where λ is the wavelength of incident light, d is the width of slit, and θ_n is the nth diffraction angle. For the porous MoO_3 film on ITO/glass with a nanocrack, it is clear that the transmitted light was more diffused and scattered, which is caused by the additionally enhanced diffractions from the scattered light on highly rough surfaces of MoO_3 films, as can be seen in Fig. 1(c).

Figure 2 shows the (a) schematic diagram of the fabrication processes for nanocracked and porous MoO_3 films on ITO/glass, (b) top-view SEM image of nanocracked hydrous and amorphous molybdenum oxide deposited by the

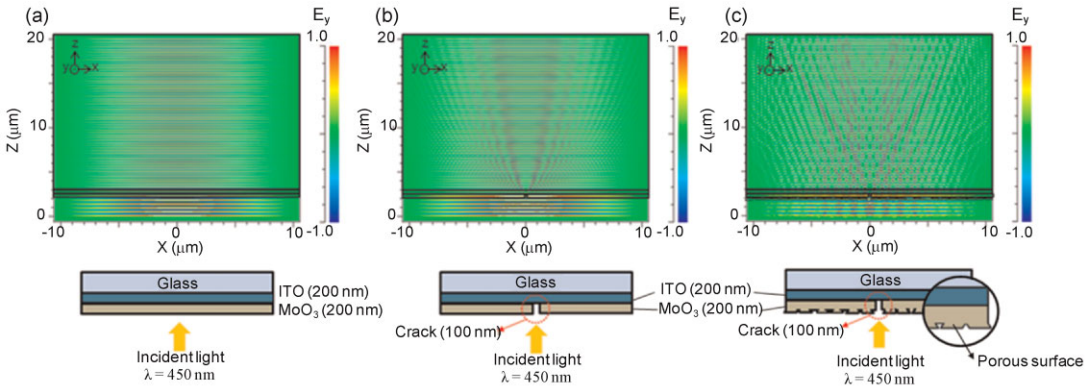

Figure 1 (online color at: www.pss-a.com) Calculated distribution of E_y passing through the (a) MoO_3 film on ITO/glass, (b) MoO_3 film on ITO/glass with nanocracks of gap distance (100 nm), and (c) porous MoO_3 film on ITO/glass with nanocracks of gap distance (100 nm).

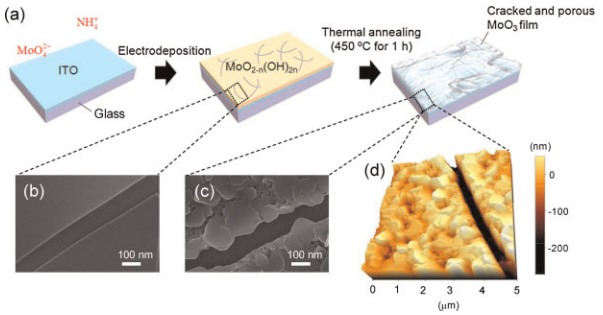

Figure 2 (online color at: www.pss-a.com) (a) Schematic diagram of the fabrication processes for nanocracked and porous MoO_3 film on ITO/glass, (b) top-view SEM image of nanocracked hydrous and amorphous molybdenum oxide deposited by the electrodeposition with an applied voltage of 2 V for 5 min, (c) top-view SEM image, and (d) AFM surface topography image of porous MoO_3 films crystallized by the thermal annealing at 450 °C for 1 h.

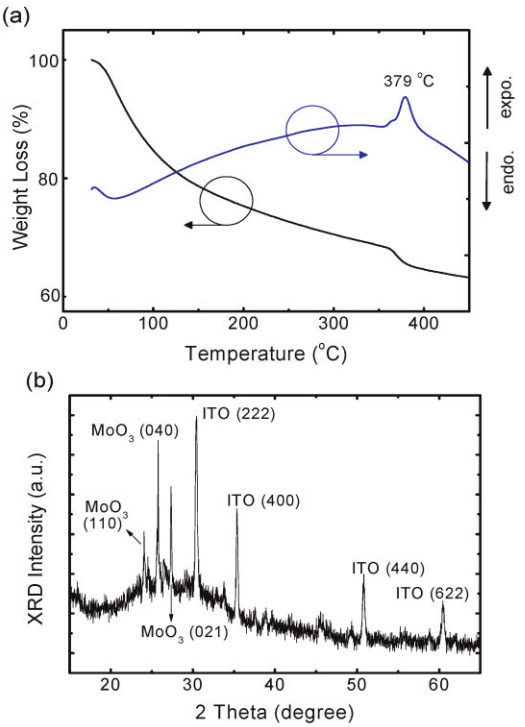

Figure 3 (online color at: www.pss-a.com) (a) Measured TGA and DTA curves in dry nitrogen atmosphere for scratched $MoO_{2-n}(OH)_{2n}$ from the deposited film ITO/glass with an applied voltage of 2 V for 5 min and (b) 2θ scan XRD pattern of the annealed $MoO_{2-n}(OH)_{2n}$ film on ITO/glass at 450 °C for 1 h under the same deposition conditions.

electrodeposition with an applied voltage of 2 V for 5 min, (c) top-view SEM image, and (d) AFM surface topography image of porous MoO_3 films crystallized by the thermal annealing at 450 °C for 1 h. When the $(NH_4)_6Mo_7O_{24} \cdot 4H_2O$ was dissolved in DI water, the MoO_4^{2-} and NH^{4+} were separated by the chemical reaction mechanism [17]. As shown in the first process of Fig. 2(a), the ITO/glass was immersed into the electrolyte containing MoO_4^{2-}, which was used for the formation of the hydrous molybdenum oxide films. In electrodeposition, a simple two-electrode system with a platinum mesh (counterelectrode) and the ITO/glass substrate (working electrode) was employed [20]. By supplying the electrons onto the surface of ITO/glass during the electrodeposition, the color was changed into transparent brown when the hydrous and amorphous molybdenum oxide films ($MoO_{2-n}(OH)_{2n}$) were formed, as shown in the second process of the schematic diagram. After rinsing the sample in DI water and drying on a hotplate at 60 °C, the uniformly deposited $MoO_{2-n}(OH)_{2n}$ films with some nanocracks (*i.e.*, narrow single slit as depicted in Fig. 1) were obtained on ITO/glass as shown in Fig. 2(b). It is noted that the drying shrinkage of $MoO_{2-n}(OH)_{2n}$ films causes the nanocracks, which can be expected to act as a narrow slit for generating efficient light diffraction [17]. By performing the thermal annealing at 450 °C for 1 h, in the third process (Fig. 2(c)), the $MoO_{2-n}(OH)_{2n}$ films with smooth surface were changed into discrete and porous films with some semihexagonal plates of MoO_3 with crystallization from hydrous MoO_2, becoming transparent. From the AFM surface topography image, high surface roughness and nanocracks with a depth of ~200 nm could be clearly observed.

Figure 3 shows the (a) measured TGA and DTA curves in dry nitrogen atmosphere for scratched $MoO_{2-n}(OH)_{2n}$ from the deposited films on ITO/glass with an applied voltage of 2 V for 5 min and (b) 2θ scan XRD pattern of the annealed $MoO_{2-n}(OH)_{2n}$ films on ITO/glass at 450 °C for 1 h under the same deposition condition. From the TGA curve, the two temperature difference regions were observed with total weight loss of 37%. The first region of temperature difference appeared from room temperature to 370 °C due to the removal of water and solvent. The second region of temperature difference was exhibited above 370 °C where the DTA curve revealed the exothermic peak at 379 °C, indicating the process of crystallization of the sample. As shown in the XRD pattern of Fig. 3(b), the (222), (400), (440), and (622) XRD peaks of the ITO were observed in the range of 2θ from 1° to 65°. The three measured XRD peaks at 24.1°, 25.8°, 27.3° mean that the $MoO_{2-n}(OH)_{2n}$ was changed into MoO_3 with preferred (110), (040), and (021) planes in the crystalline film, respectively. It is noticeable that the annealed $MoO_{2-n}(OH)_{2n}$ film on ITO/glass in air at 450 °C for 1 h is enough to provide the crystallized MoO_3 film.

In order to investigate the effect of applied voltage on the morphology and optical property of the MoO_3 films on ITO/glass, the corresponding fabrication processes in Fig. 2(a) were carried out at different applied voltages. Figure 4 shows the (i) top-view and (ii) cross-sectional SEM images of the MoO_3 films on ITO/glass at the applied voltages of (a) 1.6 V, (b) 2 V, and (c) 2.4 V. The magnified top-view SEM images of the corresponding samples were also shown in the insets of (i) of (a), (b), and (c). At the applied voltage of 1.6 V, the porous MoO_3 films were deposited on ITO/glass without

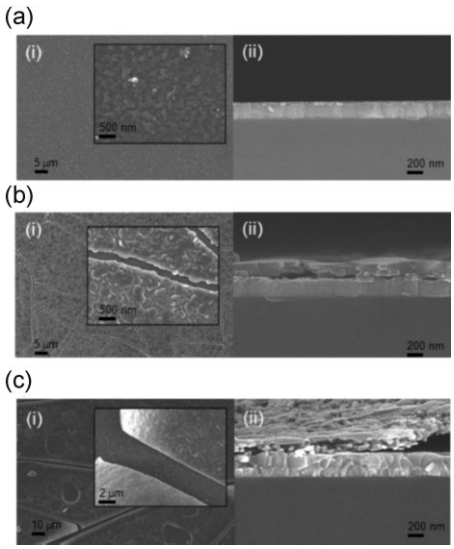

Figure 4 (i) Top-view and (ii) cross-sectional SEM images of the MoO_3 films on ITO/glass at the applied voltages of (a) 1.6 V, (b) 2 V, and (c) 2.4 V. The magnified top-view SEM images of the corresponding samples were also shown in the insets of (i) of (a), (b), and (c).

nanocracks. As shown in (ii) of Fig. 4(a), the very thin MoO_3 film of <30 nm was observed, which was not enough to produce the nanocracks because they could be created generally for the hydrous film thicker than 200 nm [21]. At the applied voltages of 2 and 2.4 V in Figs. 4(b) and (c), in contrast, the cracked surface was formed with a thickness of $\sim$200 nm. In fact, the MoO_3 was rarely deposited below the applied voltage of 1.6 V. As the applied voltage was increased from 1.6 to 2 V, however, the growth rate began to increase and it was not greatly changed between 2 and 2.4 V. In particular, the large area of nanocracks was distributed and the porous film was well coated on ITO/glass at the applied voltage of 2 V, as shown in Fig. 4(b). From the SEM image, the density of nanocrack (*i.e.* length per unit area) was microscopically estimated to approximately 1.35 μm^{-1}. At the applied voltage of 2.4 V, unfortunately, the width of cracks was further increased with less distributed area and the edge part of deposited film was somewhat lifted off as shown in (ii) of Fig. 4(c). It could be that the deposited $MoO_{2-n}(OH)_{2n}$ film, at high applied voltage, was formed with a large width of cracks on ITO/glass. Thus, under a proper applied voltage of 2 V, the density of nanocracks is expected to be controlled by varying the electrodeposition or thermal annealing time.

Figure 5 shows the three-dimensional 5 $\mu m \times 5$ μm scale AFM surface topography images and height histograms of (a) the bare ITO/glass and the electrodeposited MoO_3 films on ITO/glass with the applied voltages of (b) 1.6 V, (c) 2 V, and (d) 2.4 V. For bare ITO glass, it exhibited a smooth surface with the low root-mean-square (RMS) surface roughness of about 3.48 nm. The deposited MoO_3 thin film at the applied voltage of 1.6 V produced a relatively rough surface with an RMS roughness of 14.86 nm, as shown in Fig. 5(b). At the applied voltages of 2 and 2.4 V, the RMS surface roughness values were increased to 31.57 and 47.77 nm, respectively. By comparing the three histograms, the measured height of surface was more widely distributed with an increase of the applied voltage, which indicated a good surface morphology to provide efficient light-scattering properties. It is clear that the diffuse component and light scattering are closely related to the surface roughness and interference layers by the scalar scattering theory [22].

Figure 6 shows the total (diffuse + specular) transmittance (T_T) as a function of wavelength from 250 to 1100 nm for the MoO_3 films on ITO/glass at different applied voltages of 1.6, 2, and 2.4 V. The inset shows the diffuse transmittances (T_D) for the same samples. For comparison, the T_D and T_T of the ITO/glass were also characterized. In order to measure the T_D and T_T, the transmitted light from the sample was collected by using the integrating sphere and specular light port [20]. For the ITO/glass, the T_T of $>80\%$ was observed in the wavelength range of 500–950 nm. As the applied voltage was increased for the electrodeposition of MoO_3 film on ITO/glass, the T_T was somewhat decreased due to the reflection and absorption losses, which were induced by the Fresnel reflection and defect level in MoO_3 films, respectively [18].

As shown in the inset of Fig. 6, the ITO/glass exhibited very low T_D values of $<3\%$ in the wavelength range of

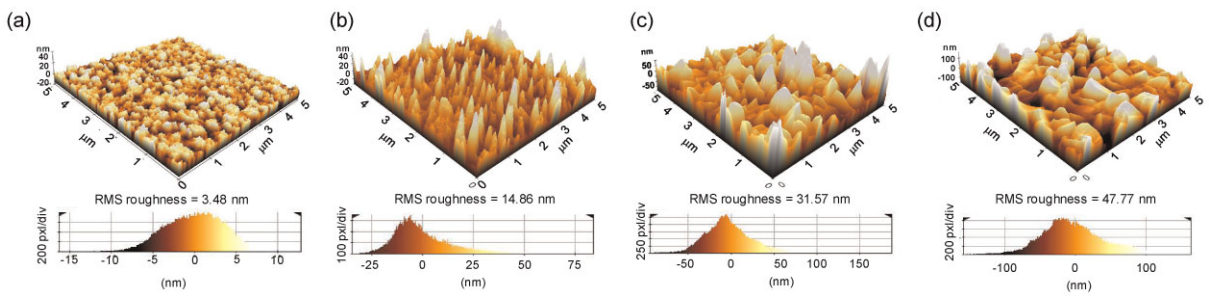

Figure 5 (online color at: www.pss-a.com) Three-dimensional 5 $\mu m \times 5$ μm scale AFM surface topography images and height histograms of (a) the bare ITO/glass and the electrodeposited MoO_3 films on ITO/glass at applied voltages of (b) 1.6 V, (c) 2 V, and (d) 2.4 V.

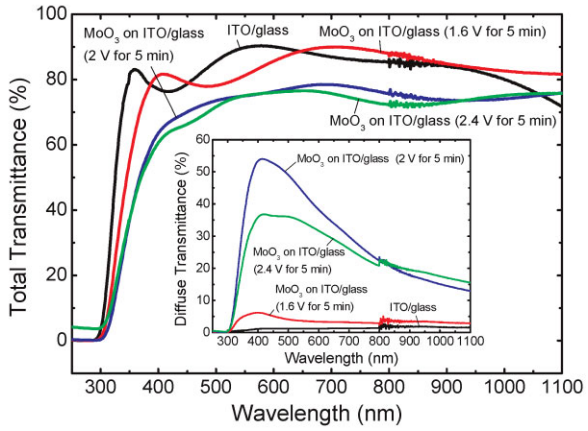

Figure 6 (online color at: www.pss-a.com) T_T as a function of wavelength from 250 to 1100 nm for the MoO_3 films on ITO/glass at different applied voltages of 1.6, 2, and 2.4 V. The inset shows the T_D for the same samples. For comparison, the T_D and T_T of the ITO/glass are also shown.

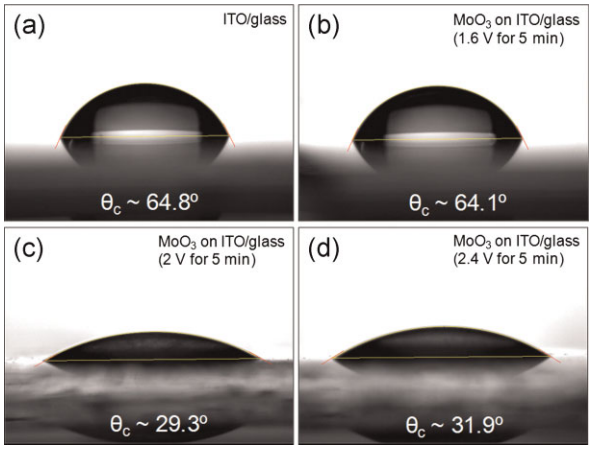

Figure 7 (online color at: www.pss-a.com) Photographs and contact angles (θ_c) of water droplets for the surface of (a) ITO/glass and MoO_3 films on ITO/glass at different applied voltages of (b) 1.6 V, (c) 2 V, and (d) 2.4 V.

250–1100 nm. This means that most photons passed directly through the sample in specular mode. When the MoO_3 film was deposited onto ITO/glass, however, the increase of T_D was observed over a wide range of wavelength. For the MoO_3 film on ITO/glass at the applied voltage of 2 V, especially, the T_D was considerably enhanced in the visible region, exhibiting the T_D value of 54% at $\lambda \sim 410$ nm. This increased T_D is caused by the light diffraction in narrow slit-like structures with a high surface roughness, leading to the enhanced diffuse light scattering [11]. Moreover, although the surface roughness of MoO_3 film deposited at 2 V was less than that at 2.4 V, the T_D of the MoO_3 film deposited at 2 V is higher than that at 2.4 V. This can be explained by the fact that the light diffraction of nanocracks is dominant at proper crack size and decreases with increased crack size for the diffuse light-scattering property, as described in the simulation results of Fig. 1.

The modification of surface wettability behavior of MoO_3 films on ITO/glass is important in an ambient environment because the surface of MoO_3 has been known to be hydrophilic [23]. Figure 7 shows the photographs and contact angles (θ_c) of water droplets for the surface of (a) ITO/glass and MoO_3 films on ITO/glass at different applied voltages of (b) 1.6 V, (c) 2 V, and (d) 2.4 V. The ITO/glass and the thin MoO_3 film on ITO/glass at the applied voltage of 1.6 V exhibited similar surface wettability of $\theta_c \sim 64.8$ and 64.1°, respectively. However, for cracked and porous MoO_3 films on ITO/glass at the applied voltages of 2 and 2.4 V, the θ_c values were decreased to be 29.3 and 31.9°, respectively, as shown in Figs. 7(c) and (d). This indicates that the hydrophilic property is greatly affected by the surface morphology of cracked and porous MoO_3 films on ITO/glass, which would be caused by the enhancement of surface roughness [24]. Therefore, the modified surface of MoO_3 films provides better water-spreading property as well as efficient light scattering. The enhanced hydrophilic surface property can be useful for environment friendly antifog transparent films [25, 26]. The nanocracked and porous surface of MoO_3 with a novel photon management may result in the improvement of optoelectronic and photovoltaic devices.

4 Conclusions The nanocracked and porous MoO_3 films were deposited on ITO/glass by the subsequent processes, including electrodeposition method and thermal annealing. When the $MoO_{2-n}(OH)_{2n}$ films were crystallized during the thermal annealing at 450 °C for 1 h in air, the cracks were self-formed with high surface roughness. Such cracked and porous morphology of MoO_3 film on ITO/glass could be expected to provide efficient diffuse light scattering by theoretical analysis using the FDTD simulations. For the MoO_3 films on ITO/glass deposited at the applied voltage of 2 V, the T_D was largely increased in the visible region and the T_D value of 54% was observed at $\lambda \sim 410$ nm. In comparison with the T_D values and morphologies of MoO_3 films at the applied voltages of 2 and 2.4 V, the amount of diffuse transmitted light was greatly affected by the light diffraction in nanocracks, which was reasonably consistent with the simulation results. Additionally, the hydrophilic surface was observed by measuring the contact angle. Consequently, the nanocracked and porous MoO_3 films on ITO/glass offered the enhanced hydrophilic surface as well as the efficient light-scattering properties, which can be useful for the antifogging and microfluidic, photovoltaic, and optoelectronic devices.

Acknowledgements This research was supported by the Basic Science Research Program through the National Research Foundation of Korea (NRF) funded by the Ministry of Education, Science and Technology (No. 2011-0026393).

References

[1] H. Bao and X. Ruan, Opt. Lett. **20**, 3378 (2010).
[2] M. Agrawal and P. Peumans, Opt. Express **16**, 5385 (2008).
[3] O. L. Muskens, J. G. Rivas, R. E. Algra, E. P. A. M. Bakkers, and A. Lagendijk, Nano Lett. **8**, 2638 (2008).
[4] S. H. Lim, W. Mar, P. Matheu, D. Derkacs, and E. T. Yua, J. Appl. Phys. **101**, 104309 (2007).
[5] K. R. Catchpole and A. Polman, Opt. Express **16**, 21793 (2008).
[6] A. Hongsingthong, T. Krajangsang, I. A. Yunaz, S. Miyajima, and M. Konagai, Appl. Phys. Express **3**, 051102 (2010).
[7] C. C. Lin, W. L. Liu, and C. Y. Hsieh, J. Appl. Phys. **109**, 014508 (2011).
[8] D. Wan, F. Huang, and Y. Wang, Appl. Mater. Int. **2**, 2147 (2010).
[9] Y. H. Ko and J. S. Yu, Opt. Express **19**, 25935 (2011).
[10] S. S. Lo, D. Haung, and D. J. Jan, Opt. Express **18**, 662 (2010).
[11] Y. H. Ko and J. S. Yu, Opt. Express **19**, 15574 (2011).
[12] A. Pennisi and F. Simone, Sol. Energy Mater. Sol. Cells **28**, 233 (1992).
[13] N. A. Chernova, M. Roppolo, A. C. Dillon, and M. S. Whittingham, J. Mater. Chem. **19**, 2526 (2009).
[14] E. Shembel, R. Apostolova, V. Nagirny, I. Kirsanova, Ph. Grebenkin, and P. Lytvyn, J. Solid State Electrochem. **9**, 96 (2005).
[15] H. Hu and I. E. Wachs, J. Phys. Chem. **99**, 10911 (1995).
[16] A. M. Taurino, A. Forleo, L. Francioso, P. Siciliano, M. Stalder, and R. Nesper, Appl. Phys. Lett. **88**, 152111 (2006).
[17] R. S. Patil, M. D. Uplane, and P. S. Patil, Appl. Surf. Sci. **252**, 8050 (2006).
[18] A. Szekeres, T. Ivanova, and K. Gesheva, J. Solid State Electrochem. **7**, 17 (2002).
[19] A. Sasaki, Jpn. J. Appl. Phys. **19**, 1195 (1980).
[20] H. K. Lee, M. S. Kim, and J. S. Yu, Nanotechnology **22**, 445602 (2011).
[21] I. Zhitomorsky and A. Petric, Mater. Lett. **46**, 1 (2000).
[22] A. Roos and D. Rnnow, Appl. Opt. **33**, 7908 (1994).
[23] W. Gulbinski, D. Pailharey, T. Suszko, and Y. Mathey, Surf. Sci. **475**, 149 (2001).
[24] R. N. Wenzel, Ind. Eng. Chem. **28**, 988 (1936).
[25] K. Guan, Surf. Coat. Technol. **191**, 155 (2005).
[26] J. A. Howarter and J. P. Youngblood, Macromol. Rapid Commun. **29**, 455 (2008).

